Study of the stability of CsI and iodine oxides (IOx) aerosols and trapping efficiency of small aerosols on sand bed and metallic filters under irradiation

Loic Bosland, Olivia Leroy, Coralie Alvarez, Mouheb Chebbi, Celine Monsanglant Louvet, Soleiman Bourrous, Karine Chevalier Jabet

Study of the stability of CsI and iodine oxides (IOx) aerosols and trapping efficiency of small aerosols on sand bed and metallic filters under irradiation

Loïc Bosland[1], Olivia Leroy[1], Coralie Alvarez[1], Mouheb Chebbi[2], Céline Monsanglant-Louvet[2], Soleiman Bourrous[2], Karine Chevalier-Jabet[1]

[1] *Institut de Radioprotection et de Sûreté Nucléaire, PSN-RES, Cadarache BP 3 – 13115 Saint Paul Lez Durance, France*

[2] *Institut de Radioprotection et de Sûreté Nucléaire, PSN-RES, Saclay BP 68 – 91192 Gif-sur-Yvette, France*

Corresponding author : Loic.bosland@irsn.fr

Abstract

The decomposition of deposited CsI and iodine oxides (IOx) aerosols deposited on sand bed and on a metallic filter has been pursued under irradiation at 120°C. On the sand, it was found that CsI aerosols are decomposed by the irradiation and the temperature effect into an inorganic specie assumed to be molecular iodine. The temperature effect might be due to surface effects of the sand grains as CsI aerosols are usually stable at this temperature. IOx aerosols are expected to be well retained by the sand filter (DF > 100) as long as the sand height is high enough (> 60 cm). IOx are also decomposed by the temperature and irradiation. The humidity is also expected to have a significant influence on their decomposition. On the metallic filter, despite both species are expected to be significantly decomposed, very few gaseous iodine release from the filter was observed. The gaseous iodine species produced by the aerosols decomposition is assumed to be quickly adsorbed on the steel wires even if a slow desorption is also expected.

Keywords

Source Term, severe accident, Cesium iodide aerosols, Iodine oxides aerosols, FCVS, sand filter, metallic filter, decomposition kinetics

Introduction

TMI (Three Miles Island) accident (1979) had led Nuclear Safety authorities to launch R&D programs whose aim was to develop and implement efficient Filtration Containment Venting System (FCVS) for Pressurized Water Reactor (PWR) and Boiling Water Reactor (BWR) in order to limit the release of Fission Products (FP) in the environment and the related short and long term consequences. In the 1980', one of the FCVS passive technologies that was studied to retain the aerosols composed of FP and structure material was the sand bed filter. As aerosols coming from Molten Corium-Concrete Interaction (MCCI) were not considered at that time, it was assumed that up to 5 kg of aerosols could be released from the containment. PITEAS program (1982-1986) [1,2,3,4] was thus launched to optimize the filtration parameters of sand bed filters (the sand particle diameter varied from 0.42 to 1.5 mm whereas the vented gas velocity ranged from 7 to 14 $cm.s^{-1}$) on intermediate scale experiments to meet the efficiency criterion of the aerosol filtration (Decontamination Factor (DF) > 10 for Cs_2CO_3 aerosols tested with $0.6 < MMAD < 1.5$ µm (Mass Median Aerodynamic Diameter)). Following Chernobyl accident (1986), sand filters have been implemented on French Nuclear Power Plants (NPPs) from 1987 to 1989 to avoid any loss of the containment integrity (by the pressure increase) and limit the ground long-term contamination (especially by ^{137}Cs) in case of accident. FUCHIA program (1990) [3,4] was then performed within the aim to validate the filtration requirements (DF > 10 for aerosols with MMAD ~ 1 µm) of the installed sand bed filters (a scale 1 of the filter was tested). Another objective of this program was to quantify the DF for gaseous I_2.

Nevertheless, the residual heat power brought by the radioactive aerosols and FPs on the sand filter (that is located outside the reactor building) could be important and might (1) prevent some safety actions to be pursued because of the high dose brought by the FP on the sand and (2) lead to a delayed re-volatilization of gaseous compounds in the environment. It was thus designed a Metallic Filter (MF) whose aim was to ensure, inside the containment building, an efficient pre-filtration of aerosols (with a requirements of DF > 10 for aerosols) before the gas is sent to the sand bed filter. From 1990 to 1993, additional tests were performed in order to

optimize the design of MFs [3,4]. They were installed inside the reactor building of the French NPPs from 1992 to 1995, at the venting inlet so that the global required DF (MF + sand filter) for aerosols was expected to be over 100. However, the MF has been designed considering a maximum FP aerosol mass of 5 kg suspended in the containment [3]. Nevertheless, if the MCCI aerosol production is considered, the aerosol mass on the MF could increase by one order of magnitude (≈ 50 kg). To prevent the blockage of the venting system by MCCI aerosols clogging, a by-pass has been added to the MF in order to send the over-pressured containment gas to the sand filter (with no pre-filtration) thanks to a by-pass valve that would open as soon as the pressure drop on the MF would reach 1 bar. As a consequence, this could thus limit the overall DF for aerosols in the venting line and could bring a significant aerosol mass (including FP) on the sand filter.

These researches have led to quantify aerosol DF higher than 10 for the MF and higher than 100 for the sand filter which should provide an overall DF higher than 1000 for aerosols if the MF is not clogged. Once on the MF or on the sand filter, iodine aerosols (like iodine oxide aerosols and iodine multicomponent aerosols containing cesium) would be exposed to (1) the radiation field brought by the FPs, (2) to the temperature (~ 140°C) and (3) to water vapors. Such iodine aerosol stability in these conditions is not precisely known. However, it has been shown recently that under irradiation, IOx and CsI aerosols deposited on surfaces are not stable in similar temperature conditions [5] (CsI being usually assumed to be the main representative iodine aerosol entering the containment from the reactor coolant system). If the conditions on the MF and the sand filter are strong enough to lead to the decomposition of IOx and multicomponent iodine aerosols, it is expected that molecular iodine would be one of the main products of the decomposition reactions (organic iodides may also be formed in the sand filter). It was recently found that gaseous I_2 (and CH_3I) are not well retained neither by the MF ($DF(I_2) \approx 10$, $DF(CH_3I) = 1$) nor by the sand filter ($DF(I_2, CH_3I) \approx 1$ [6]. Another result from FUCHIA program [3] (on a scale 1 sand bed filter) was that, even though I_2 is not trapped by the sand itself, it could be adsorbed on the steel surfaces of the line and on the deposited aerosols on the steel/sand surfaces, leading to an estimated $DF(I_2)_{line} \approx 10$. It is thus expected that any gaseous inorganic and organic iodine compounds coming either from the containment or from the decomposition of iodine aerosols trapped on the MF or the sand filter would be partially or totally released to the environment though the venting line. The quantification of how much gaseous iodine could be released from the MF and the sand filter to the environment is thus crucial for the source term determination. This quantification has

been performed within the MIRE (2013-2019) and PASSAM [7,8] (2013-2016) projects in which IOx and CsI aerosol stability on such devices has been checked. As IOx aerosol size was found to be smaller (MMAD < 0.5 µm [9]) than (1) the aerosol size used to qualify the aerosols DF in FUSCHIA project and (2) the iodine multicomponent aerosol size quantified in PHEBUS-FPT0/1 containment (MMAD > 1 µm [10]), DF of IOx on the sand filter has thus been reevaluated using a simulant (impaction experiment). The results of these experiments are presented in this article.

1 Description of the geometry of the metallic filter and sand bed filter

The MFs (**Fig. 1**) installed on the French NPPs is a PALL® Corporation product [4]. It consists of 92 filtering elements of 800 mm length and 60 mm diameter each [6,11], with a total filtration geometrical surface of 33 m². These filtering elements, called "cartridges", are made, from the internal to the external parts, by: (1) a perforated internal grid; (2) a metallic weaved supporting layer; (3) a first filtering metallic medium (PFM FH 200); (4) a second filtering medium (PFM 40) and (5) a metallic weaved protective layer (Cf. left parts of **Fig. 4** and **Fig. 3**).

The sand bed filter installed on each French NPPs [4] is a thermally insulated cylindrical device filled with 6.5×10^4 kg of sand [11], set up (most of the time) on the roof of a nuclear island building. This filter (**Fig. 1**) has the following characteristics: total height 4 m; internal diameter 7.3 m; geometrical filtering area 42 m²; sand layer thickness 0.8 m [3].

2 Description of the experiments

Different experiments (thermal and under irradiation) were carried out to check CsI and IOx aerosols stability. The thermal decomposition tests were performed with crystalline CsI powder or with CsI aerosols deposited on sand (at 1 bar) in dry and humid air (the tests conditions are recapped in **Table 1**. The irradiation tests were performed in EPICUR facility (**Fig. 7**) with iodine aerosols (CsI, IOx) deposited on sand or on a MF. Their characteristics are summarized in **Table 2**. Complementary tests were also performed to evaluate the DF of fine particles (whose size is representative of iodine oxides aerosols) deposited on sand bed filter

(cf. **Table 3**) in SOFA and CATFISH facilities. More details are given below for each type of experiment.

2.1 Description of the experimental devices

2.1.1 Sand bed filter

The sand installed on NPPs has an average particle diameter close to 0.6 mm. We have thus chosen a SIBELCO HN 0.4/0.8 (from Hostun in Isere Valley, France) sand product to perform our studies as the granulometry ranges from 0.5 to 0.7 mm with no pre-treatment. Its composition is shown on **Table 4**. The sand was introduced in a 125.6 cm^3 steel cylinder equipped with two flanges in order to setup the gas circulation under irradiation (**Fig. 2**). The sweeping gas arrives on the top of the sand cylinder and leaves it by the bottom. The water content in the sand (stored at room temperature) was estimated (by mass difference after having been dried in an oven for 48 hours) to be around 2 wt%. As all the pre-irradiation phases lasted from 2.0 to 6.5 hours, and as the gaseous residence time in the steel cylinder ranges from 10 to 20 seconds, we assume that the steam equilibrium is quickly reached in the sand after the beginning of SF2 and SF4 (with a relative humidity (RH) = 30%) and that the sand humidity is quickly removed from the sand for SF1 and SF3 (dry tests).

2.1.2 Metallic filter

The filter used is a PALL Corporation product (PFM40+PFM200, porous metal fibre). The cartridge was cut by electro-erosion in several cylindrical sections (60 mm diameter and 52 mm length representing a geometrical surface of 96 cm^2) and equipped with two flanges to allow a gas injection during the irradiation as shown on **Fig. 3**. It is made of a cylindrical made with two steel filtration sheets (**Fig. 4**) inserted between two gauzes representing with a geometrical filtration surface of 0.36 m^2 per cartridge. The sheets are ~ 1 mm thickness and are made with steel wires and have an 85% porosity.

2.1.3 Aerosols filtration (SOFA test)

The objective of these tests is to check the efficiency of the sand bed filter to efficiently trap small size particles (MMAD < 0.5 µm) like IOx. Uranine aerosols were employed to do so.

Uranine aerosol production is obtained by atomization of a solution of fluorescein sodium ($C_{20}H_{10}Na_2O_5$, ref. RAL-313160-0100, purity 98.44%) according to the standard NF EN ISO 16170 [12] to get an aerosol Mass Median Diameter (MMD) of 0.15 µm. In a first step, the solution droplets are sent to a series of impactors in order to select only a certain range of droplets size. Then, the droplets are dried to get the final fluorescein dry aerosols whose size is quantified with a scanning mobility particle sizer (SMPS). The SMPS leads to the determination of the MMD that is centered on 0.18 µm (with Geometric Standard Deviation $1.5 < GSD < 1.7$). Considering a fluorescein density of $\rho = 800$ kg.m^{-3}, it corresponds to a MMAD = 0.16 µm ($MMAD = MMD.(\rho/\rho_0)^{0.5}$ with $\rho_0 = 1000$ kg.m^{-3}) with the same GSD.

The SOFA test bench (**Fig. 5**) is used to perform these filtering efficiency tests. The sample holder has an internal diameter of 30 mm. The air flow rate through the column is controlled at 5.87 Nl.min^{-1}. The whole filtration device is regulated at 80°C. The temperature could not be set up at a higher value as fluorescein sodium is known to degrade for higher temperatures (it would then led to a degraded optical yield and concentration). The influence of the temperature on the aerosols filtration (from 80 to 140°C) is not expected to be significant. In fact, the only parameters that could influence the aerosol filtration are the gas density and the time residence of the aerosols in the sand filter. These two parameters are not expected to be significantly modified for higher temperatures, so that the results obtained at 80°C are assumed to be independent on the temperature in the expected temperature range of interest (80-200°C). The RH is controlled at 15% through a syringe containing water that is slowly pushed through a heating resistance to control the humidity. This low humidity is representative of the expected RH on the sand bed and will avoid the steam condensation. Experimental conditions are recapped in **Table 3**. The decontamination factor of the filter is obtained by the ratio between the upstream concentration ($C_{upstream}°$) and downstream concentration ($C_{downstream}$) (Eq. 1):

$$DF = C_{upstream}°/ C_{downstream} \qquad \text{(Eq. 1)}$$

Both concentrations were determined by a UV spectrophotometer. A wavelength of 490 nm is used to excite the fluorescein molecules. Then, they reemit a typical fluorescein 520 nm wavelength whose calibration allows to determine the fluorescein concentration which means that all particles (whatever their size) are quantified.

The test duration is either 20 min, either 40 min in **Table 6**. Even though the downstream concentration and the DF depend on the sand height, it is assumed that the DF is independent of the upstream concentration, on the humidity (as long as there is no steam condensation) and temperature.

2.2 Choice of the experimental conditions

Experimental conditions are recapped in **Table 2** and **Table 5**. The choice of the temperature and RH of the tests is discussed below. In order to estimate all the temperatures and RH ranges that could be found on the sand filter, ASTEC [13,14] sensitivity studies were performed on two calculations for a 900 MWe PWR to estimate a range of gas temperature and RH that could be found in the containment. Considering a 3 and 12 inches break in the hot leg of the Reactor Coolant System (RCS), with no security injection and no aspersion available, the results show that, within the first day of the accident, the containment temperature can range between ~ 140°C (short term) and ~ 200°C (long term) and that the containment RH can vary between 30-75 % (short term, 5 bars) and 15-58 % (2.8 bars after one day of depressurization) for more than 90 % of the calculated scenarii.

According to the specifications of the filter [1], the gas temperature coming from the reactor building is expected to be close to 140°C (for a pressure of 5 bars that slowly decreases all along the transient). A pre-heating phase of 20 hours at 140°C is also supposed to be performed before the opening of the venting procedure in order to avoid steam condensation in the line (upstream the sand filter).

Before the containment gas arrives to the sand filter, a pressure relaxation is performed with a relief device so that the pressure of the gas reaching the sand filter is close to 1.1 bars. Such phenomenon should lead to a limited temperature decrease as the sand filter was pre-heated and is insulated (but not temperature controlled). The PITEAS tests have shown that even if the gas temperature being injected on the insulated and pre-heated pipes is 135°C, the sand temperature ranges from 111 to 135°C depending on the test conditions [15] which corresponds to $14\% < RH < 25\%$ (for $0.35 < X_{H2O(mass)} < 0.68$). For our tests, we have chosen to set up a 120°C temperature in order to consider, on one hand, the pressure relaxation before the sand bed that is supposed to slightly lower the gas temperature coming from the containment, and on the other hand, the heat losses through the non-controlled temperature

insulated pipes walls. This temperature is also in the upper range of the temperature that can be reached in the laboratory.

In the FUCHIA tests, the range of temperatures measured in the sand filter varied significantly as 115°C < T < 200°C (upper range taking into account the residual power of the deposited FP in the sand and highest gaseous temperature expected in the containment). As the mass fraction of steam is 65% (75% molar), it corresponds to 5 % < RH_{FUCHIA} < 50%.

It is well known that CsI and IOx aerosols are hygroscopic. For IOx, steam leads to the conversion of dry IOx species (like I_4O_9, I_2O_5, I_2O_4) into hydrated forms of IOx species [16,17] (like HIO_3 and HI_3O_8). For CsI, a water shell is expected to form around CsI aerosols. However, it is not known the effect of the humidity of IOx and CsI aerosol decomposition under irradiation. For a reactor containment, as the venting procedure leads to a depressurization from 5 bars to ~ 1.1 bars and assuming a sand bed filter temperature range 115°C < T < 200°C, we can consider that the RH on the sand filter can be comprised between 2% (minimum corresponding to a water vapor mass fraction $X_{H2O(mass)}$ = 0.32 at 200°C) and 65% (maximum corresponding to a water vapor mass fraction $X_{H2O(mass)}$ = 1 at 115°C) in most of the results (~ 95 % of the calculations) even if we expect the main scenarii to lead to 10% < RH < 30% (for 0.32 < $X_{H2O(mass)}$ < 1.0 for an average temperature of 140°C on the sand).

The influence of the RH on CsI and IOx aerosols decomposition was thus checked at 0 and 60 % in order to cover this range of RH expected on the sand filter.

The gas flow rates used in these laboratory tests are lower than the highest expected values representative of the beginning of the releases when the depressurization line is open. Some technical limitations of the facility prevented to use representative values for this short term releases. They are nevertheless considered relevant for the longer terms for which the gas flow rate in the line is expected to decrease (because of the pressure decrease in the containment).

2.3 Thermal decomposition tests description

The set-up for thermal decomposition tests is presented on Fig. 6. A glass column containing the sample is heated to the desired temperature, a flow of dry or humid gas passes through the sand column towards alkaline liquid traps. In the first test series (PCsIEAS and PCsIEAH1), the commercial CsI crystalline powder (Acros Organics 99.9%) is deposited on the bottom of the glass column in order to reach a height of 2 cm of crystalline CsI. The initial crystalline CsI mass is thus not well quantified (no sand was used in these two tests). This commercial CsI powder was chosen to complete our previous studies of the decomposition of deposited CsI/CdI_2 aerosols on stainless steel that showed no CsI/CdI_2 decomposition at 105°C and 120°C respectively [19].

As soon as the desired temperature is reached, the carrier gas is injected, from the bottom of the column, with dry or humid air. The tests duration is 23h. The sampling in the scrubbers is made once an hour and analysed by ICP-MS. At the end of the test, the CsI powder is taken out of the column for storage and a sodium hydroxide solution (0.1 $mol.L^{-1}$) is used to lixiviate the pipes and the reactor in order to calculate the mass balance.

In the second test series (TD1 and TD2), CsI aerosols were generated with a CsI powder (Acros Organics 99.9%) dissolved in an aqueous solution ([CsI] = 10 g/l, MMAD ≈ 0.8 ± 0.1 µm, c.f. next section for the GSD). An aerosol generator (PALAS® GmbH device referenced AGK 2000) is used at room temperature to get CsI aerosols. The gas injection flow rate in the CsI solution is performed with a pump. At the end of the dryer, a U shaped pipe leads to the deposition of CsI aerosols on the top of the sand located in a steel cylindrical tank (the initial deposited aerosols CsI mass on the sand is known with a 10-15 % uncertainty). After loading, the sand with deposited CsI aerosols is manually emptied into a glass column ($Ø_{internal}$ = 2 cm, sand height 25 cm), leading to get CsI aerosols not only on the top of the sand but mixed with the sand. The column is then heated to 120°C. As soon as the desired temperature is reached, the carrier gas is injected with dry or humid air from the top of the column. The sampling in the alkaline scrubbers is made regularly and analysed by ICP-MS. At the end of the test, the sand with CsI is taken out of the column for lixiviation with a sodium hydroxide solution (0.1 $mol.L^{-1}$) as well as the pipes and the glass column in order to calculate the iodine and caesium mass balance.

As these tests were performed at P = 1 bar and 120°C, RH = 60% could not be reached (as for the tests under irradiation). It would have led to steam condensation as the partial steam pressure for RH=60% and 120°C is over 1 bar. Moreover, in order to get the steam to the CsI powder location, a continuous air gas flow has to be set up which tended to limit the amount of steam that could be used in these kind of experiments. That is why RH = 30% was set up in these thermal decomposition tests.

Moreover, even though the reference conditions to evaluate the effect of the humidity are not the same (RH = 30% without irradiation and RH = 60% with irradiation), the amount of steam at RH = 30% is high enough and in large excess towards the initial CsI deposited mass. We thus assume that if steam has a thermal effect, it should be seen for RH = 30%.

2.4 Irradiation tests description

A series of six tests were performed in the EPICUR facility to evaluate the medium and long terms behaviour of iodide aerosols under irradiation previously deposited respectively on the sand bed filter (SF1 to SF4) and on the MF (MF1).

2.4.1 Iodine aerosols generation and deposition on the filters

For SF1 and SF2 tests, CsI aerosols are generated in the same way as for thermal decomposition tests, using a CsI concentration of 10 g/L in the aqueous solution and a 125.6 cm^3 steel cylinder tank filled with sand. It leads to polydisperse CsI aerosols with a MMAD ≈ 0.8 ± 0.1 µm and with a geometric standard deviation GSD ≈ 2.3 ± 0.1 µm.

For MF1 test, a MF is present in the cylindrical tank and the aqueous CsI concentration had to be increased to 120 g/L (leading to polydisperse CsI aerosols with MMAD ≈ 1.5 ± 0.1 µm and with a geometric standard deviation of σ_g ≈ 2.3 ± 0.1 µm). In addition, $Na^{131}I$ is added to the solutions in order to label the generated CsI aerosols (NaI aerosols are also generated but Na concentration is very low compared to Cs concentrations as the ratio Cs/Na is higher than 5700 and 130 000 for SF and MF tests respectively). After aerosol loading and γ counting, the filter (sand on **Fig. 2** and metallic **Fig. 3**) is equipped with two flanges (in order to inject the gas under irradiation) and set up in the irradiation vessel. This specific design allows a

homogeneous face velocity of the sweeping gas: from the top to the bottom for the sand bed filter and radially from the outside to the inside for the MF.

For SF3, SF4 and MF3 tests, Iodine oxide aerosols (IOx) are produced by direct oxidation between ozone and gaseous molecular iodine. Gaseous molecular iodine is formed through the following aqueous reaction ($Na^{131}I$ being used label the molecular iodine produced in the solution) (R1):

$$5\ I^- + IO_3^- + 6H^+ \Rightarrow 3\ I_2 + 3\ H_2O \qquad (R1)$$

I_2 is then transferred to the gaseous phase and sent to a glass reactor (IOx reactor) in which ozone is injected thanks to an ozone generator. An aerosol fog, composed of fine white IOx particles, is formed instantaneously. These labelled iodine oxide aerosols are transferred to another reactor to be deposited on the sand bed filter or MF. Both steps occurs in a few minutes. As for CsI tests, after aerosol loading and γ counting, the filter is equipped with two flanges (for the gas circulation) and inserted in the irradiation vessel.

2.4.2 EPICUR facility

EPICUR facility has been described elsewhere [18]. Briefly, it deals with an irradiator with six ^{60}Co sources ($T_{1/2}$ = 5.27 years, representing an activity of 893 TBq as of September 2012), an irradiation vessel and a gas loop transporting the gaseous labelled iodine species towards a May-pack device composed of selective filters and allowing online measurements by γ counting. Thus, the three volatile species of iodine (aerosol, molecular and organic iodine) that might exist in the irradiation vessel are continuously monitored. The average dose rate at the level of the CsI aerosols deposited on the coupon is close to 1 $Gy.s^{-1}$ (**Table 2**). **Fig. 7** gives the general scheme of the EPICUR facility. The different volatile iodine species released during the tests are transferred to the May-pack device and trapped on the different filters of this device. The configuration of the May-pack for all the tests is the following one: One quartz fiber filter (1QF) is intended to aerosols trapping followed by two stages composed of three Knit-mesh filters (2KM1, 2KM2, 2KM3 - 3KM1, 3KM2, 3KM3) for molecular iodine trapping. The fourth stage composed of three TEDA (Ethylene-diamine-tetra-acetic) impregnated activated carbons filters (4CA1, 4CA2, 4CA3) is intended for all

others species, particularly organic iodides in our experiments. However, the activity fixed on the FQ filter could also be attributed to adsorbed I_2 (parasitic trapping), at least partially. Thanks to the use of ^{131}I to label the iodine species, on-line measurements allow the evaluation of the release kinetics of the different volatile species during the tests. After each test, the irradiation vessel and the loop are leached in order to recover and to measure, as far as possible, iodine quantities trapped reversibly in the various surface and to quantify the activity balance. It was checked the stability of two kinds of compounds:

- CsI aerosols stability under irradiation was checked on two types of substrates: sand (SF1 and SF2 tests) and the MF (MF1 test). For SF2, a heat insulating deficiency of the sweeping gas injection line was observed. It led to a temperature gradient in the sand that is estimated to have ranged from 100 (upper part) to 110°C (lower part). As a consequence, it led to a RH estimated to range between 100 % (top of the sand vessel where the temperature is the lowest) and 80 % (bottom of the sand vessel where the temperature tends to approach the targeted temperature) instead of a 60 % RH targeted value. It might have led to water condensation on the upper part of the vessel. In addition, to avoid a too important gaseous iodine adsorption on the surface of the loop (it has been observed a 14.2% iodine inventory in the rinsing solution of SF1 test), the internal pipes of the loop were renewed before SF2 was performed which has led to lower down the activity of the SF2 rinsing solution to 2.9%.

  Around 10 mg of iodine was deposited on the sand filter under the CsI aerosol form whereas 195 mg (iodine mass of CsI aerosols) were deposited on the MF to increase the measurements precision. Thermal tests were also performed to check the influence of the temperature.

- For IOx aerosols stability study, sand (SF3 and SF4) and the MF (MF3) were also tested. Around 1 mg of iodine was deposited on the sand filter under the IOx aerosol form and irradiated for ~ 30 hours at 120°C with no humidity or 60% RH.

For the SF tests, the dose rate was comprised between 0.61 $Gy.s^{-1}$ and 0.86 $Gy.s^{-1}$ whereas it is comprised between 0.39 $Gy.s^{-1}$ and 0.72 $Gy.s^{-1}$ for MF tests.

3 Results and discussion

3.1 Uranine filtration Efficiency on sand bed filter

The test conditions are presented on **Table 3** and the results are presented in **Table 6** and **Fig. 8**. The results of DF obtained (with an uncertainty of ± 5%) at different sand heights show a correlation of the filtration efficiency as a function of the thickness of the sand bed. For a maximum height tested of h = 80 cm, the DF obtained is 443 ± 26. The results are consistent with those obtained in the 1990's in the FUCHIA facility for which DF was found to be higher than 100 for aerosols [3]. In Fig. 8, even if the uncertainty on the DF quantification is important (± 30%), the FUCHIA results show a significant DF difference for a similar sand height. Despite the aerosols used for the 0.60 granulometry sand are bigger (MMAD ≈ 2 µm) and might have led to a higher DF than for the 0.58 granulometry sand (with MMAD ≈ 1 µm), the smallest granulometry sand is found to be more effective to trap the smallest aerosols (MMAD ≈ 1 µm). This difference was mostly explained by the sand granulometry that was slightly different: 0.58 mm for DF = 506 (MMAD ≈ 1 µm) and 0.60 mm for DF = 148 (MMAD ≈ 2 µm) leading to less spaces between the sand grains for the 0.58 mm sand granulometry. Moreover, the sand with the lowest granulometry had been pack down, leading to a decrease of 3 cm of its height. We thus expect the sand with the 0.58 mm granulometry to have been more compact than the sand with the 0.6 mm granulometry, which in turns is expected to have contributed to a better trapping of the aerosols (MMAD ≈ 1 µm), and thus, to a higher DF. The influence of a wider range of particles size and composition on the DF was not pursued but it would be interesting to do so in order to complete the identification of the main parameters influencing the trapping efficiency and quantify their effect. The FUCHIA program (1989-1992), which used a full scale replica of the sand bed filter, was performed to qualify the filtering efficiency with relevant thermal-hydraulic parameters. The FUCHIA facility included representative carbon steel pipes from inside the containment up to the plant chimney, the sand bed filter but the MF trapping efficiency was not tested.

3.2 CsI decomposition on the sand filter

3.2.1 Decomposition of CsI without irradiation: influence of the temperature and humidity

Blank tests (no irradiation) were performed to check the influence of the temperature on the decomposition of CsI. Two kinds of tests were performed with: (1) crystalline CsI powder (no

sand, test PCsIEAS and PCsIEAH1) and (2) deposited CsI aerosols on sand (tests TD1 and TD2).

Crystalline CsI powder does not decompose at 120°C (for duration test > 20h) whatever the RH checked (0 and 30%) in Table 1. This is consistent with previous results dealing with the study of the thermal decomposition of CsI aerosols deposited on steel and quartz coupon [19] at similar temperatures. However, when CsI is deposited on sand under an aerosol form (≠ powder), a significant thermal decomposition occurs as 15-20 % of the iodine initial inventory is released on Fig. 9 for a test duration time > 66 hours. A similar thermal release is observed during the initial thermal phase of SF1 (6.5 hours, 120°C, 0% RH) on Fig. 10 before the irradiation starts. For SF2 (100-110°C), the release observed during the first 3 hours (dry air) is more important than SF1 despite similar initial conditions (Table 1). The main differences between SF1 and SF2 are the temperature and the presence of humidity. However, SF2 temperature is lower than for SF1 which should have led to a lower CsI decomposition. The mechanism involved in this decomposition is thus not obvious. In SF2, the steam injection from 3 to 5 hours before the irradiation starts does not seem to influence CsI decomposition as for SF1. Moreover, CsI decomposition on sand stops after a certain time (Fig. 9) as a steady-state is observed for the iodine release.

As no Cs was found in the alkaline scrubbers, no volatile Cs species were formed at such temperature so that we assumed that the main iodine released specie is inorganic. Moreover, for both test series (TD and PCsIEA), as no caesium was found in the alkaline solution, no CsI resuspension or remobilisation (caused by air flow) occurred during the thermal test.

Moreover, SF1 and SF2 tests show that the main iodine release is trapped on the knitmesh part of the maypack filter all over the test which confirms the inorganic nature of the iodine volatile release.

According to **Fig. 9**, the humidity does not have a significant influence for RH ranging from 0% to 30% which seems to indicate that water molecule do not have any influence on CsI decomposition. The free energy of CsI reaction with water at 25°C is shown below (R2):

$$CsI + H_2O \leftrightarrow CsOH + HI \qquad \Delta G_r°(298K) = +166\ kJ.mol^{-1}\ (+189) \qquad \text{(R2)}$$

CsI decomposition by water is not possible at 25°C and it is not likely that a significant decomposition would occur at 100-120°C which is consistent with the observation of previous studies without sand [19]. Another explanation has thus to be found for the thermal release. According to Zhuravlev [20], the SiO_2 surface of the sand is hydroxylated so that the surface is covered with Si-OH and Si-$(OH)_2$ groups as long as T < 400°C. Even if no steam was injected in TD1 test, it is possible that the surface Si–OH groups might play a major influence on CsI decomposition at 120°C for TD1 and TD2 tests. It suggests (1) a modification of the CsI speciation that would lead to one stable specie whose speciation is not identified or (2) a total consumption of the Si-OH groups on the surface of the sand particle accessible to CsI that would prevent the complete decomposition of CsI aerosols.

It is thus likely that the hydroxylated groups (Si-OH) of the sand particle surface might play a significant effect on CsI thermal decomposition with a limitation given by the accessibility of CsI particles to Si-OH groups.

3.2.2 CsI radiolytic decomposition: effect of the relative humidity

For SF1, after the irradiation starts (> 3h, indicated by vertical dotted lines on **Fig. 10**), there is no slope modification, suggesting that the irradiation has an insignificant effect on CsI decomposition in dry conditions. This is also confirmed by the post-irradiation release (after 31h). In dry conditions, CsI decomposition seems to be driven by a thermal decomposition mechanism despite the irradiation.

For SF2, the slope decrease significantly as soon as the irradiation starts (> 3h) and it is observed that the slope of the release under irradiation is similar for SF1 and SF2. For both tests, a post-irradiation release is still observed with a similar rate to the one of the irradiation phase.

The irradiation has a different effect for both tests and needs to be clarified as the tests conditions are rather similar. The humidity is the only significant different parameter that could be one cause of these differences. However, another phenomena explained below might also contribute to explain this observation.

3.2.3 Influence of the loop replacement on the Iodine trapping on the Maypack

As the pipes of the loop were replaced between SF1 and SF2, a discussion is made below to evaluate this modification on the release shown on **Fig. 10**. The rinsing solution of SF1 (including the loop washing) highlighted a 14.2% contribution to the iodine activity balance whereas a 2.9% contribution was observed for SF2 which indicates that the surface state of the SF1 loop might have been more degraded, leading to a higher iodine trapping on the steel of the loop. For both tests, ≈ 15% of the iodine inventory is lost in the activity balance and is assumed to be adsorbed on the steel surfaces of the vessel and the loop. The correction made on the on-line inorganic data assumes a homogeneous addition of the missing activity balance and the washing contribution all over the test. However, for SF1, it is possible that a higher CsI thermal degradation could have occurred during the first hours of the test and that the loop surfaces might have retained/adsorbed more volatile I_2 than for SF2 for which the loop was new. We thus assume that the SF1 loop state surface might have been degraded by previous tests so that the beginning of gaseous iodine release could have been preferentially trapped in the loop rather than transferred to the Maypack. The SF1 thermal release is thus expected to be underestimated on **Fig. 10**.

3.2.4 Mechanisms of CsI aerosol thermal decomposition on sand particles

CsI aerosols are known to be thermally stable on quartz and steel surfaces [19]. However, they decompose when they are deposited on sand particles. If the sand surface plays a significant influence on CsI decomposition, the following surface mechanisms leading to CsI decomposition into inorganic iodine (I_2, HOI) could occur (R3 to R8):

$$2CsI + SiOH \rightarrow CsOH + SiCs + I_2 \quad (R3)$$
$$2CsI + 2SiOH \rightarrow 2CsOH + 2Si + I_2 \quad (R4)$$
$$2CsI + 2Si(OH)_2 \rightarrow 2CsOH + 2SiO_2 + I_2 \quad (R5)$$

$$CsI + SiOH \rightarrow SiCs + HOI \quad (R6)$$
$$CsI + 2Si(OH)_2 \rightarrow Si(OH)Cs + HOI \quad (R7)$$
$$CsI + 2SiOH \rightarrow CsH + SiOSi + HOI \quad (R8)$$

As a result, two gaseous compounds could be formed: molecular iodine (I_2) and hypoiodous acid (HOI) could be formed. In EPICUR facility, the Maypack is composed of the knit-mesh part dedicated to trap molecular iodine as it is made of copper wires covered with silver. As silver is very reactive with iodine, I_2 is quickly and efficiently trapped on the knit-mesh stage. It is also expected to be partly adsorbed on the surfaces of the loop which could explain the missing activity balance (up to ≈15%). If HOI was formed during the test, as it is not known to react with silver, it would have been transferred to the charcoal filter on which it is not known to be trapped either [21]. The mechanism leading to the thermal decomposition of CsI on the sand remains to be identified.

3.3 IOx aerosols decomposition on the sand filter

3.3.1 Effect of the relative humidity

SF3 test was performed in a dry atmosphere. No significant on-line gaseous release was observed (1.8% were recovered in the washing solutions of the vessel and loop in **Table 7**) whereas a significant release was observed on **Fig. 11** for SF4 (performed in similar conditions with a 60% RH). The role of the humidity seems to be crucial in the decomposition process of IOx into volatile iodine under irradiation.

3.3.2 Interpretation

The volatile gaseous iodine release really starts after 17 hours (15 hours of irradiation). A "blank thermal test" (call IOx1, no irradiation) was performed at the same temperature (120°C) and a similar humidity (50%RH), IOx being deposited on a flat quartz coupon rather than on sand. It also highlighted that IOx aerosols start to decompose ~ 10 hours after the beginning of the test. This observation is not well understood at this stage but it could correspond to the time necessary for IOx to hydrate and be converted into a species that can be decomposed at this temperature. After IOx formation at room temperature, RAMAN analyses were performed and they have shown that the main specie is expected to be I_2O_4. However, at the time of starting the irradiation tests, this initial speciation can be modified significantly by the presence of steam and by temperatures higher than 75-80°C according to the following chemical mechanisms (R9 to R18) [16,17,22,23,24,25,26]:

Hydration mechanisms leading to HIO_3 specie

$$5I_2O_4 + 4H_2O \leftrightarrow 8HIO_3 + I_2 \quad (R9)$$
$$5I_4O_9 + 9H_2O \leftrightarrow 18HIO_3 + I_2 \quad (R10)$$
$$3I_2O_5 + 3H_2O \leftrightarrow 2I_2O_5 - HIO_3 + 2H_2O \leftrightarrow 6HIO_3 \quad (if\ R.H > 40-60\%) \quad (R11)$$
$$I_2O_5 + H_2O \leftrightarrow 2HIO_3 \quad (R12)$$

Conversion mechanisms due to the temperature

$$5I_2O_4 \leftrightarrow 4\,I_2O_5 + I_2 \qquad 85-100°C < T < 130°C \qquad (R13)$$
$$4I_4O_9 \leftrightarrow 6\,I_2O_5 + 2I_2 + 3O_2 \qquad 75-85°C < T < 125°C \qquad (R14)$$
$$5I_4O_9 \leftrightarrow 9\,I_2O_5 + I_2 \qquad 142°C < T < 190°C \qquad (R15)$$
$$2I_2O_5 \leftrightarrow 2I_2 + 5\,O_2 \qquad 280°C < T < 350°C \qquad (R16)$$
$$2HIO_3 \leftrightarrow I_2O_5 - H_2O \qquad T > 70°C \qquad (R17)$$
$$I_2O_5 - H_2O \leftrightarrow I_2O_5 + H_2O \qquad T > 200°C \qquad (R18)$$

As a result, IOx speciation at the beginning of the tests could be I_2O_5, I_2O_4 and HIO_3 or a combination of these species as all of these are stable at room temperature.

According to several studies, the hydration processes could take from one to several hours [17,27] and would lead to HIO_3 specie. This duration is compatible with the time constants observed in SF4 and the thermal blank test (IOx1) and indicate that HIO_3 might be the main IOx species that decomposes into volatile iodine after a certain irradiation time (~ 15 hours in our conditions).

Moreover, Little *and al.* [28] found that I_2O_5 react with alcohol solution and leads to the formation of volatile I_2 with the following mechanism (R19):

$$I_2O_5 + 10ROH \rightarrow 5H_2O + 10RO + I_2 \qquad (R19)$$

A similar mechanism (R20) could also occur with HIO_3:

$$2HIO_3 + 10ROH \rightarrow 6H_2O + 10RO + I_2 \qquad \text{(R20}$$

As sand surface is composed of silanol groups (Si-OH and Si-$(OH)_2$), similar mechanisms (where R = Si) could occur on its surface. It would contribute to the release of volatile iodine in absence of radiation.

3.4 Effect of the metallic filter on CsI and IOx aerosols decomposition

Even if a significant (or complete) CsI aerosols decomposition was expected under irradiation from previous data obtained from steel and quartz surfaces [19], it wasn't observed any significant on-line gaseous release on the Maypack filter. Nevertheless, some activity was found on the rinsing solutions of the vessel and the loop (~ 8.5% of the iodine inventory) which highlights a significant gaseous iodine release. CsI aerosols are also expected to be decomposed significantly by the irradiation in these conditions. A reliable explanation for the low iodine amount detected on the Maypack could be that molecular iodine formed by CsI aerosols decomposition would be adsorbed by the steel wires as on steel surfaces (and leading to physisorbed and chemisorbed iodine species) [29,30]. As the MF is made with steel wires (316 L) whose developed cylindrical surface is estimated to range between 1 and 10 m^2, gaseous iodine formed by CsI aerosols decomposition could have been adsorbed on the wires surface. A calculation was performed with ASTEC V2.1 [31] in order to check if the surface developed by the stainless steel could be high enough to adsorb molecular iodine formed by CsI decomposition. Considering that the wires state surface is probably not electro-polished, we expect a higher adsorption rate on the metallic wires of the filter than in previous publications dealing with electro-polished steel surfaces [32,33]. Sensitivity studies were performed and have shown that if we consider a steel surface available for I_2 adsorption from 1 to 10 m^2, the adsorption rates compatible with these experimental results range from 10^{-4} to 10^{-3} $m.s^{-1}$ and the desorption rate from 10^{-6} to 10^{-5} s^{-1}. These rates are compatible with previous publications [32, 33, 34] on iodine interaction with steel as they are from one to two orders of magnitude higher than the ones expected for electro-polished steel (and for which the interaction of gaseous iodine is expected to much be slower). It is also compatible with the first part of this work [6] for which it was found that, at 100°C and 35% RH, gaseous I_2 was retained on the MF with a DF ≈ 10 (i.e. 90% retention in 4 hours).

For IOx aerosols, MF3 test has also shown a low amount of iodine on the Maypack (8.1% of the initial activity). A similar process than for CsI is expected: IOx aerosols are expected to be significantly decomposed by the effect of the temperature and irradiation, leading to significant gaseous I_2 formation. The large surface of the steel wires is expected to significantly trap I_2 (or another inorganic iodine gaseous species) before it has a chance to be sent to the Maypack.

As soon as gaseous iodine is trapped on the MF, a slow desorption process has been observed at 100°C (40% RH) [6] which indicates some potential delayed releases to the sand filter that does not retain volatile iodine species. More tests should be performed in order to assess whether other conditions (like higher temperatures or humidities) would favour I_2 retention or revolatilization from the MF.

For all tests, a low amount or organic iodides has been detected on the Maypack, even before the irradiation starts (< 1% of the inventory). It could be due to organic pollutants that can react with iodine under irradiation and/or a small quantity of inorganic iodine that is not retained by the knitmesh filter of the Maypack.

3.5 Modeling of the data with ASTEC

In a previous publication [19], we addressed the modeling of deposited CsI aerosols decomposition on surfaces under irradiation. This model considered the only influence of the irradiation as no temperature effect has been observed. On sand grains, as explained before, a surface effect (possibly depending on the temperature) is likely and would require more data to set-up an appropriate model in ASTEC. Moreover, the aerosols expected to come from the containment are multicomponent (and most probably insoluble), so that their decomposition probably undergo a different kinetics that should be foreseen.

For IOx aerosols, a decomposition model is under development for IOx deposited on coupons and will be published and compared to the SF4 data to check whether it is also valid for IOx aerosols decomposition in the sand filter.

No decomposition model for CsI/IOx aerosols deposited on the MF has been set up because most of the iodine inventory is retained by the filter.

4 Conclusions and perspectives

Uncertainties used to remain about the stability of the deposited/trapped aerosols by sand filters and MFs. The stability of CsI and IOx aerosols on sand filter and MF has thus been pursued to better evaluate the source term following an activation of the depressurization procedure in case of severe accident.

For the sand filter, it was found that the filtration of small aerosols like IOx (MMAD < 0.5 µm, produced in the containment) by the sand filter depends on the sand height (h) and is expected to be efficient (DF > 100) for h > 60 cm. However, IOx aerosols are not stable and decompose under the effect of the temperature, humidity and irradiation. Some gaseous inorganic iodine delayed releases are thus expected if IOx aerosols reach the sand filter. Soluble CsI aerosols have been chosen as a representative aerosols composition to simulate the multicomponent aerosols coming from the RCS (and agglomerating in the containment). CsI aerosols have been found to decompose in the sand under the effect of the irradiation. A thermal decomposition process has also been observed and could be due to a surface effect between the aerosols and the sand grains that would participate to decompose CsI aerosols into volatile inorganic iodine.

For the MF, despite a significant expected decomposition of IOx and CsI aerosols, a low gaseous iodine amount was recovered downstream the filter. The large surface developed by the steel wires of the filter are expected to efficiently trap the gaseous inorganic iodine formed by their decomposition even though slow and low delayed gaseous inorganic iodine releases to the sand filter may be expected, especially in the short term when higher gas flow rates than those used are expected in the depressurization line. However, in case the MF is by-passed, IOx and CsI aerosols coming from the containment would be transferred to the sand filter on which they are not stable.

These tests have been performed in a relatively restricted range of conditions (temperature, humidity and dose rate). Other sets of these parameters would also be interesting to pursue in

order to better evaluate their influences on the source term. Moreover, both type of studies were performed with soluble aerosols (IOx and CsI). A more complete evaluation could also be performed considering a non-soluble aerosol (like AgI) or a metallic multicomponent aerosol in order to check whether their behaviour is different and better evaluate the implications for the source term evaluations.

As a result, the decomposition of iodine aerosols into volatile iodine in the depressurization line of power plants has to be considered in the source term evaluations.

Acknowledgments

Authors acknowledge the French Government through the "Investissements d'Avenir" program managed by the National Research Agency (ANR) for supporting MIRE project (grant agreement N° ANR-11-RSNR-0013-01) and the MIRE partners for their support (Aix-Marseille Université, Framatome, CNRS, Electricité de France, IRSN, Université de Lorraine, ARMINES, Université Lille 1). Authors also want to thank the European Atomic Energy Community (Euratom) for supporting the PASSAM project in the frame of the 7th framework program FP7/2007-2013 under the grant agreement n° 323217 and the PASSAM partners (AREVA, CIEMAT, CSIC, Electricité de France, IRSN, PSI, RSE, VTT and Université de Lorraine).

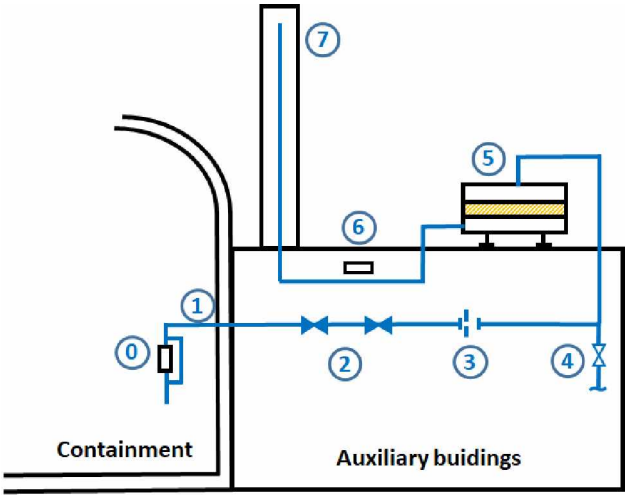

Fig. 1: General view of the metallic filter and sand filter ((0) : metallic filter and its by-pass, (1) : crossing of the containment towards auxiliary buildings, (2) : isolation valves, (3) : pressure relief device, (4) : air preconditioning/pre-heating device, (5) : sand filter, (6) : activity monitoring device, (7) : release chimney)

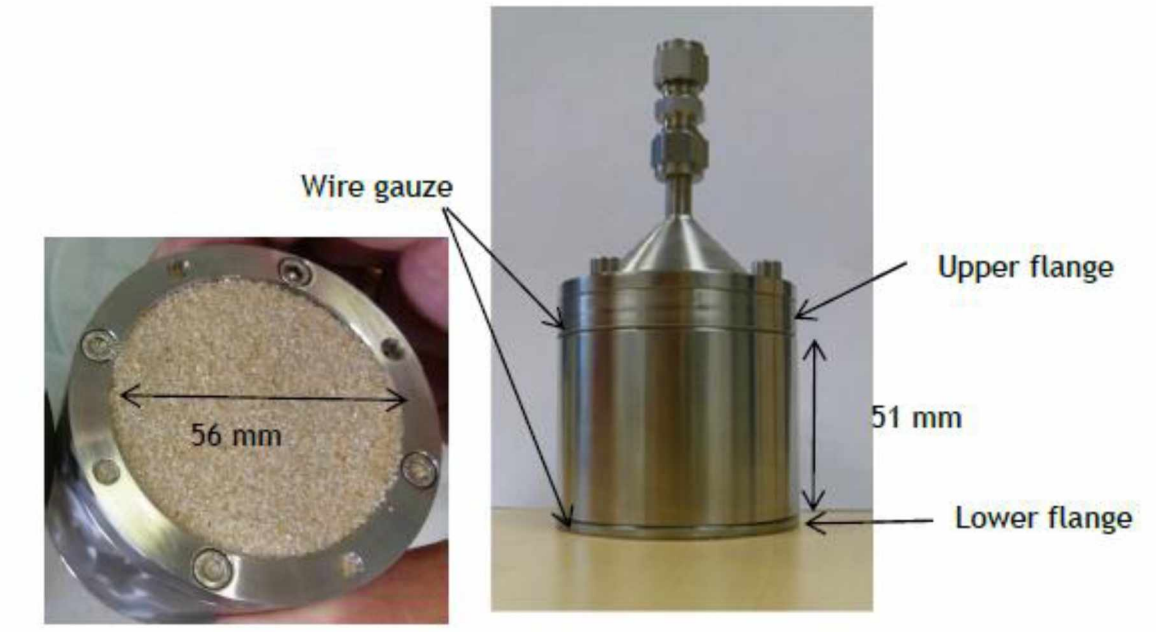

Fig. 2: picture of the sand filter used to test (with air circulation) CsI and IOx decomposition under irradiation

Fig. 3: cartridge section (52 mm length) of the MF (left) equipped with flanges for irradiation (right)

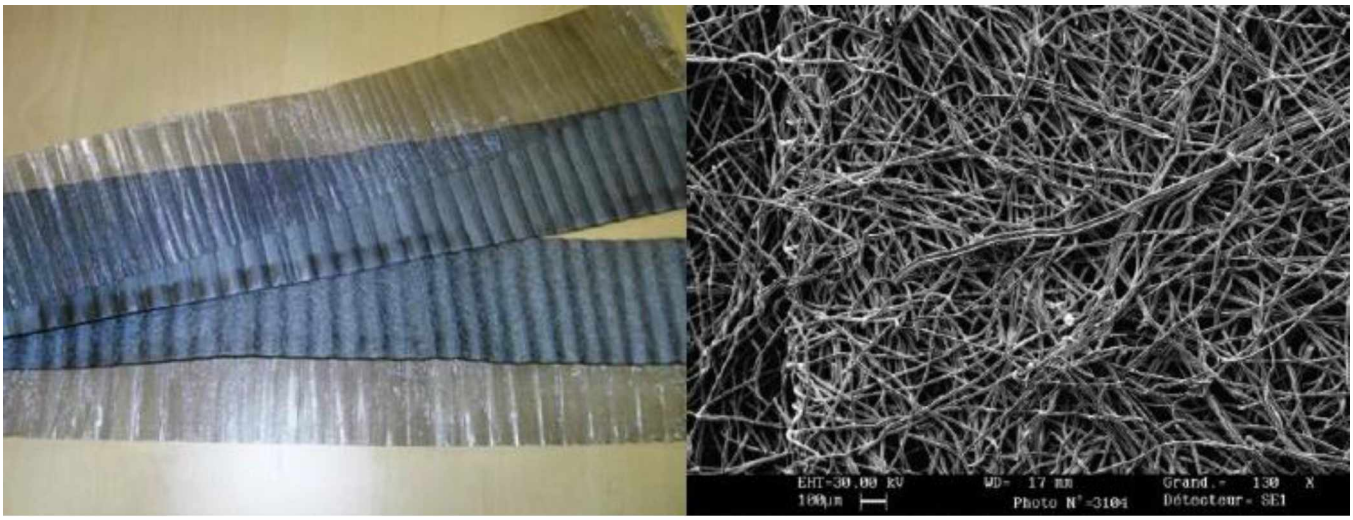

Fig. 4: picture of the steel sheets and gauzes of the filter (left) – MEB picture of the material (right)

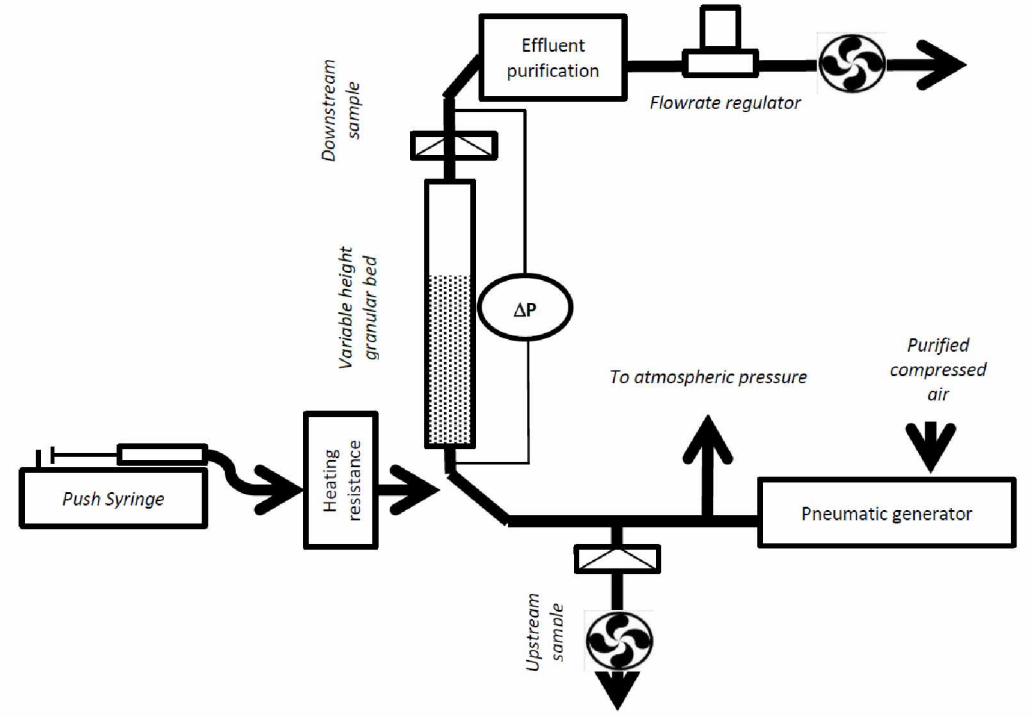

12

13 **Fig. 5**: schematic view of SOFA test bench

14

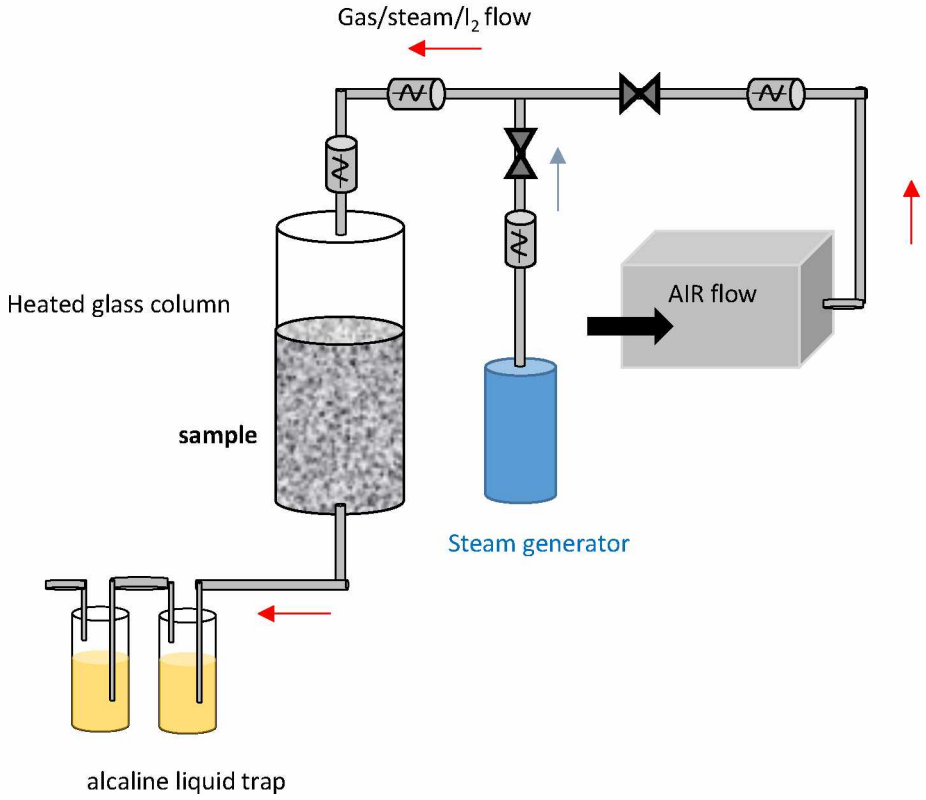

Fig. 6: thermal decomposition tests set-up

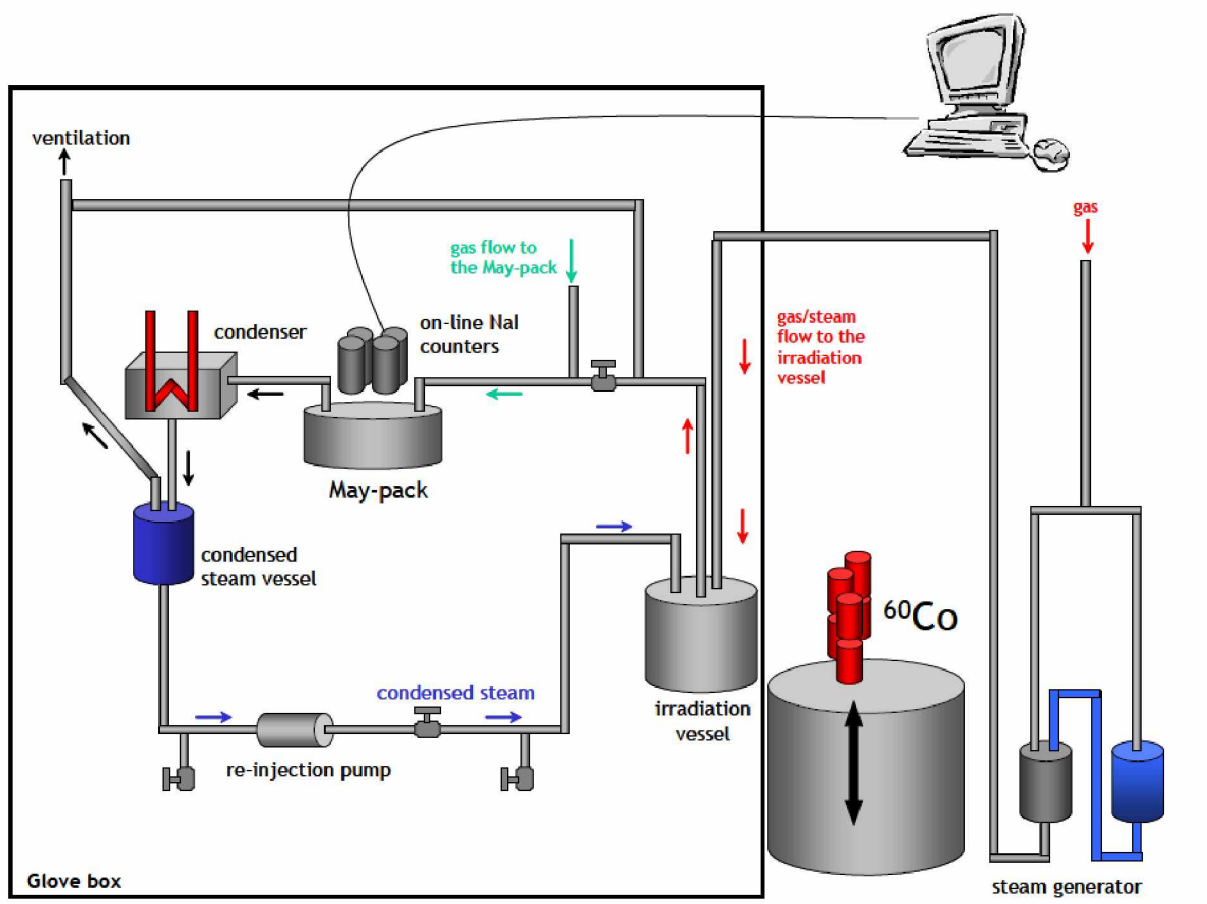

Fig. 7: simplified view of the experimental EPICUR facility

Table 1: experimental conditions of CsI thermal decomposition tests performed at P = 1 bar (no irradiation)

Test name	CsI type	Substrate	Sand mass (g)	Deposited CsI initial mass (mg)	Temperature (°C)	R.H. (%)	Gaseous flow rate in the column ($L.min^{-1}$)	Test duration (hours)	Studied parameter
PCsIEAS	Crystalline	Glass column (no sand)	/	26975 ± 200	120 ± 4	0	0.190 ± 0.002	27	Reference test (no steam)
PCSIEAH1				24367 ± 200	120 ± 4	30 ± 2	0.190 ± 0.002	23	Humidity
TD 1	Aerosol	Glass column	145.2 ± 0.2	27.7 ± 2.8	120 ± 4	0	0.190 ± 0.002	145	Reference test (no humidity)
TD 2			145.0 ± 0.2	34.9 ± 3.5	120 ± 4	30 ± 2	0.190 ± 0.002	70	Humidity

Table 2: experimental conditions of the tests performed in EPICUR facility under irradiation

Test name	Iodine aerosol species	Substrate	Sand mass (g)	Deposited initial Iodine mass (mg)	Average dose rate ($Gy.s^{-1}$)	Pressure (absolute bars)	Temperature (°C)	R.H. during irradiation (%)	Gaseous flow rate in the vessel ($L.min^{-1}$) (and duration in hours)	Studied parameter
SF1	CsI	Sand	199.9 ± 0.2	11.5 ± 1.1	0.86 ± 0.17	1.90 ± 0.10	120 ± 3	0	0.63 ± 0.01 (36.5 h)	Reference test
SF2			200.0 ± 0.2	9.3 ± 0.9	0.80 ± 0.16	3.40 ± 0.10	100-110 ± 3	80-100 ± 4	0.34 ± 0.01 (3 h) 0.26 ± 0.01 (28 h) 0.34 ± 0.01 (3 h)	Humidity
SF3	IOx		196.8 ± 0.2	1.1 ± 0.1	0.67 ± 0.13	3.50 ± 0.10	120 ± 3	0	0.34 ± 0.01 (36 h)	Reference test
SF4			198.7 ± 0.2	0.98 ± 0.09	0.61 ± 0.12	3.50 ± 0.10	120 ± 3	60 ± 4	0.35 ± 0.01 (46 h) 0.34 ± 0.01 (1 h)	Humidity
MF1	CsI	Metallic filter	/	195.0 ± 19.0	0.72 ± 0.14	3.50 ± 0.10	120 ± 3	60 ± 4	0.35 ± 0.01 (3 h)	Reference test
MF3	IOx			1.6 ± 0.2	0.39 ± 0.10	3.50 ± 0.10	120 ± 3	60 ± 4	0.25 ± 0.01 (40 h) 0.35 ± 0.01 (2 h)	

Table 3: testing conditions for the test made on the SOFA test bench.

Sample height (mm)	Sand mass (g)	Regulated temperature (°C)	RH at the beginning of the test (%)
20 ± 2	19.0 ± 0.1	80 ± 5	17.2 ± 0.1
100 ± 2	101.0 ± 0.5	80 ± 5	16.1 ± 0.1
300 ± 2	317.0 ± 1.6	80 ± 5	16.7 ± 0.1
600 ± 2	629.0 ± 3.1	80± 5	17.7 ± 0.1
800 ± 2	782.0 ± 3.9	80 ± 5	16.3 ± 0.1

Table 4: sand composition used in the SF tests

Material (SIBELCO, HN 0.4/0.8)	**Composition (%)**
SiO_2	98.94
Fe_2O_3	0.069
Al_2O_3	0.348
CaO	0.047
K_2O	0.16

Table 5: duration of the three phases of the EPICUR tests

Test	Duration of the pre-irradiation phase (hours) (no irradiation)	Duration of the irradiation phase (hours)	Duration of the post-irradiation phase (hours) (no irradiation)
SF1	6.5 (dry air)	25 (dry air)	5 (dry air)
SF2	3 (dry air) + 2 (RH = 80-100 %)	24 (RH = 80-100 %)	2 (RH = 80-100 %) + 3 (dry air)
SF3	3 (dry air)	25 (dry air)	8 (dry air)
SF4	2 (RH = 60 %)	38 (RH = 60 %)	6 (RH = 60 %) + 1 (dry air)
MF1	3 (dry air) + 8 (RH = 60 %)	28 (RH = 60 %)	4 (RH = 60 %) + 2 (dry air)
MF3			

Table 6: decontamination factor (DF) for Uranine nanoparticles (SOFA facility)

Height of the sand sample	2.0 ± 0.1 cm	10.0 ± 0.1 cm	30.0 ± 0.1 cm	60.0 ± 0.1 cm	80.0 ± 0.1 cm
Test duration (min)	20	20	20	40	40
DF	6.36 ± 0.25	15.5 ± 0.6	75.1 ± 3.2	193 ± 8	443 ± 26
ΔP experiment (Pa)	969	2270	3497	6922	8740

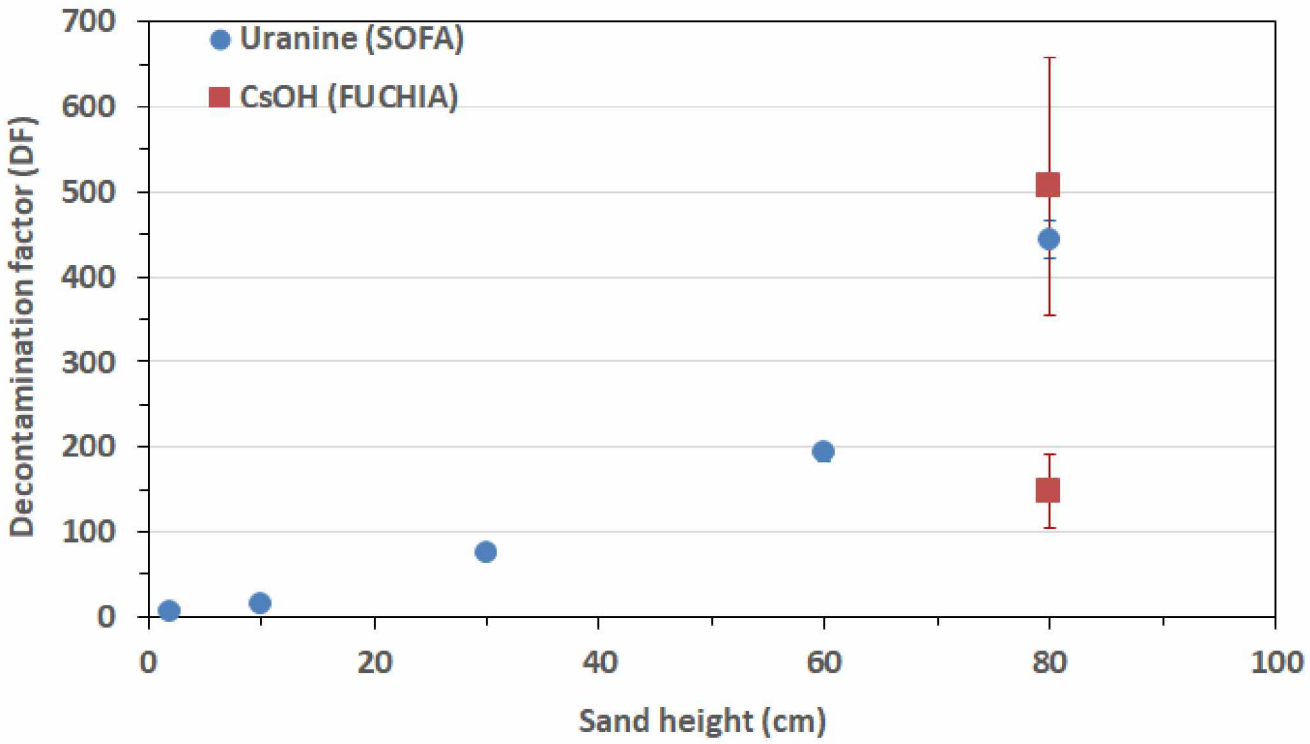

Fig. 8: evolution of the decontamination factor (DF) as a function of the height of sand for FUCHIA (CsOH aerosols, size centered on MMAD ≈ 1 µm (DF = 506) and MMAD ≈ 2 µm (DF = 148) and SOFA (Uranine aerosols, size centered on MMAD ≈ 0.18 µm) tests

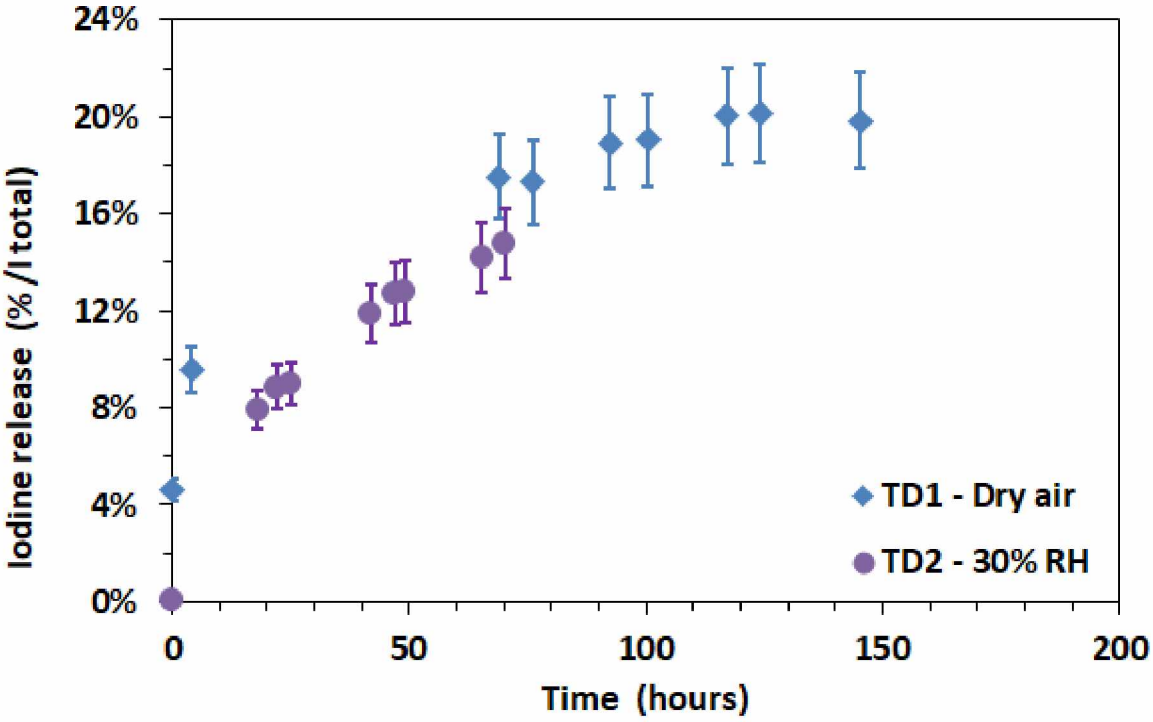

Fig. 9: evolution of the iodine release as a function of time from CsI aerosols deposited on sand (tests TD1 and TD2) at 120°C (MMAD ≈ 0.8 ± 0.1 µm)

Table 7: results of the tests (final corrected on-line measurements are in percentages (%))

Test name	Iodine aerosol species	Substrate	Studied parameter	Activity Balance (%)	Global volatilization (%)	Final corrected on-line RI (%)	Final corrected on-line I_2 (%)
SF1	CsI	Sand	Reference test	84.7 ± 5.5	42.5 ± 6.4	0.5 ± 0.1	42.1 ± 5.5
SF2			Humidity	84.0 ± 6.1	61.4 ± 16.0	1.0 ± 0.1	60.2 ± 6.2
SF3	IOx		Reference test	100.0 ± 2.0	1.8 ± 2.3	0.5 ± 0.01	1.8 ± 0.1
SF4			Humidity	99.4 ± 1.2	35.0 ± 0.5	0.7 ± 0.1	33.5 ± 1.7
MF1	CsI	Metallic filter	Reference test	104.8 ± 4.0	3.7 ± 0.2	0.020 ± 0.002	9.5 ± 0.9
MF3	IOx			94.9 ± 7.6	8.1 ± 0.8	2.6 ± 0.3	6.6 ± 0.7

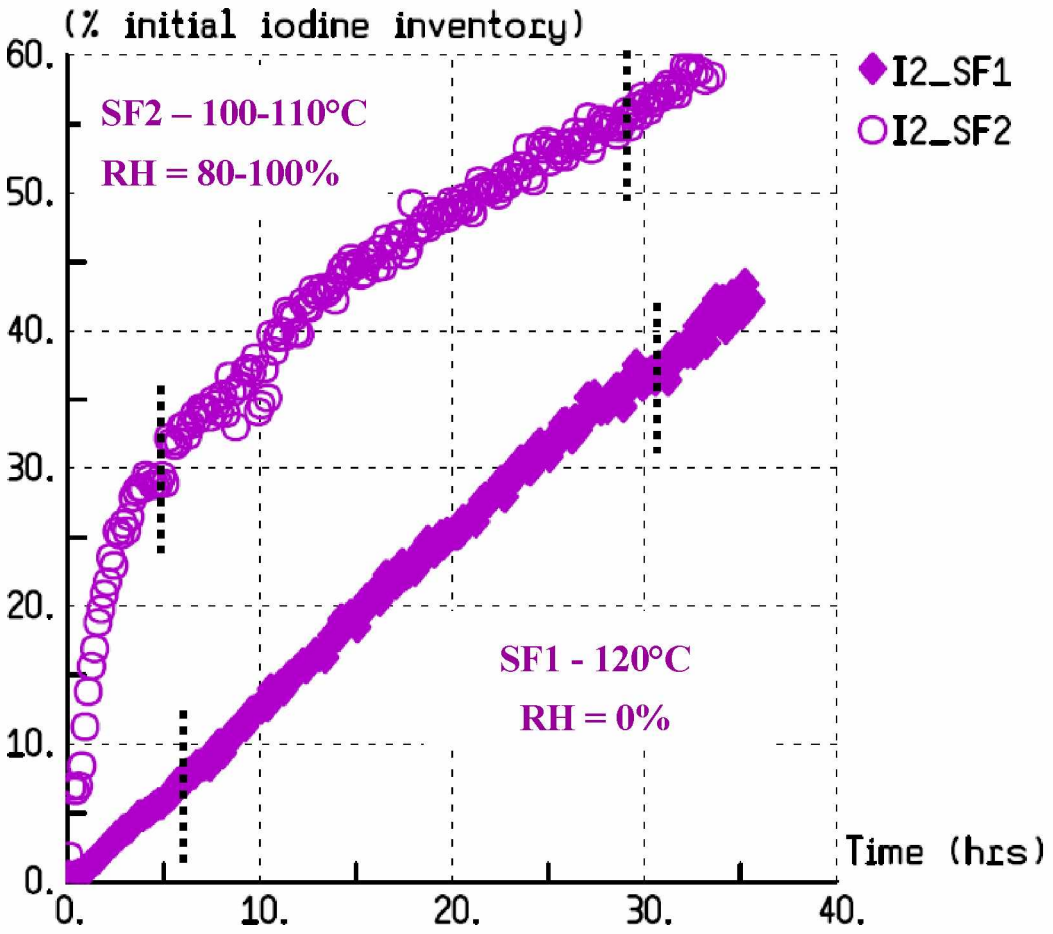

Fig. 10: CsI aerosols decomposition under irradiation (MMAD ≈ 0.8 ± 0.1 µm) - Comparison of the corrected inorganic release on the knit-mesh filter for SF1 test (0 % humidity, 120°C) and SF2 test (80-100% humidity, 100-110°C) (Vertical dotted lines indicate the beginning and the end of the irradiation)

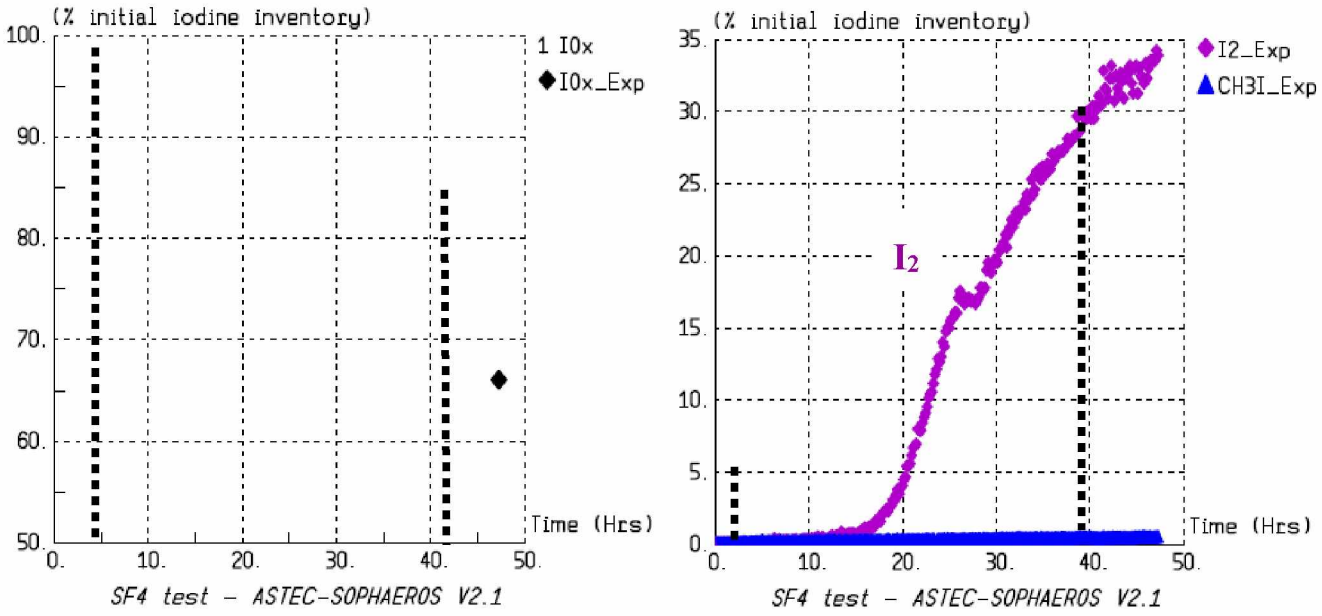

Fig. 11: SF4 test: decomposition of IOx aerosols deposited on the sand filter at 120°C and 60% RH - Remaining IOx amount on the sand filter (left) and corrected inorganic and organic release on the Maypack filter (right, vertical dotted lines indicate the beginning and the end of the irradiation)

References

1 S. Guieu; A. Couvrat-Desvergnes; M. Berlin and J. Dufresne, "Système de decompression-filtration des enceintes", IAEA-SM-296/15 - Proc. of an Int. Symposium on Severe Accidents in Nuclear Power Plants - Vol. 2, p. 255-273, March 21st-25th, Sorrento, Italy (1988)

2 V. Saldo; E. Verloo and A. Zoulalian, "Study on aerosol deposition in the PITEAS vessel by settling, thermophoresis and diffusiophoresis phenomena", J. Aer. Sci., 29 (Suppl. 2), p. 1173-1174 (1998) (https://dx.doi.org/10.1016/S0021-8502(98)90769-8)

3 S. M. Guieu, "French NPPs filtered containment venting design", 33rd Nuclear Air Cleaning Conference, June 22nd-24th, Saint Louis, MO, USA (2014)

4 OECD/NEA/CSNI, "OECD/NEA/CSNI Status report on filtered containment venting", NEA/CSNI/R(2014)7 (2014)

5 L. Cantrel; T. Albiol; L. Bosland; J. Colombani; F. Cousin; A. C. Gregoire; O. Leroy; S. Morin; C. Mun; M. N. Ohnet; S. Souvi; H. Vidal; C. Monsanglant-Louvet; B. Azambre; F. Louis and C. Volkringer, "IRSN R&D Actions on FP Behaviour for RCS, Containment and FCVS in Severe Accident Conditions ", ICONE 24, Paper 61104, June 26th-30th, Charlotte, NC, USA (2016)

6 O. Leroy, C. Monsanglant-Louvet, "Trapping measurements of volatile iodine by sand bed and metallic filters", J. Radio. and Nucl. Chem., 322, p. 913-922 (2019) (https://doi.org/10.1007/s10967-019-06786-1)

7 T. Albiol; L. Herranz; E. Riera; C. Dalibart; T. Lind; A. Del Corno; T. Kärkela; N. Losch and B. Azambre, "The European PASSAM project: R&D outcomes towards enhanced severe accident source term mitigation", ICAPP 2017, A New Paradigm in Nuclear Power Safety, April 24th-28th, Kyoto, Japan (2017)

8 T. Albiol; L. Herranz; E. Riera; C. Dalibart; T. Lind; A. Del Corno; T. Kärkela; N. Losch; B. Azambre; C. Mun and L. Cantrel, "Main results of the European PASSAM project on severe accident source term mitigation", Annals of Nuclear Energy, 116 p. 42-56 (2018) (https://doi.org/10.1016/j.anucene.2018.02.024)

9 S. Dickinson; A. Auvinen; Y. Ammar; L. Bosland; B. Clément; F. Funke; G. Glowa; T. Karkela, D.A. Powers; M. Reeks; S. Tietze; G. Weber; S. Zhang, "Experimental and modelling studies of iodine oxide formation and aerosol behaviour relevant to nuclear reactor accidents" Annals of Nuclear Energy 74: 200-207 (2014) (http://dx.doi.org/10.1016/j.anucene.2014.05.012)

10 M. Kissane, "On the nature of aerosols produced during a severe accident of a water-cooled nuclear reactor", Nucl. Eng. Des., 238, 2792-2800 (2008) (http://dx.doi.org/10.1016/j.nucengdes.2008.06.003)

11 OECD/NEA/CSNI, "OECD/NEA/CSNI Status report on filtered containment venting", NEA/CSNI/R(2014)7 (2014).

12 Norme ISO 16170 : 2016 : Méthodes d'essai in situ pour les systèmes filtrants à très haute efficacité dans les installations industrielles (2016)

13 K. Chevalier-Jabet, F. Cousin, and al., "Source term assessment with ASTEC and associated uncertainty analysis using SUNSET tool", Nucl. Eng. & Des., 272, 207-218 (2014) (https://doi.org/10.1016/J.NUCENGDES.2013.06.042)

14 P. Chatelard, S. Belon, and al., "Main modelling features of ASTEC V2.1 major version", Annals of Nuclear Energy, 93, 83-93 (2016) (http://dx/doi.org/10.1016/j.anucene.2015.12.026)

15 S. Guieu; A. Couvrat-Desvergnes; M. Berlin ; J. Dufresne, "Système de decompression-filtration des enceintes", IAEA-SM-296/15 - Proc. of Int. Symposium on Severe Accidents in Nuclear Power Plants - Vol. 2, p. 255-273, March 21st-25th, Sorrento, Italy, (1988)

16 M. W. Chase, "NIST-JANAF Thermochemical tables for the iodine oxides", J. Phys. Chem. Ref. Data, 25 (5), p. 1297-1340 (1996)

17 D. K. Smith; M. L. Pantoya; J. S. Parkey and M. Kesmez, "The water-iodine oxide system: a revised mechanism of hydration and dehydration", RSC Adv., 7 p. 10183-10191 (2017) (https://dx.doi.org/10.1039/c6ra27854jrsc.li/rsc-advances)

18 L. Bosland and J. Colombani, "Study of iodine releases from Epoxy and Polyurethane paints under irradiation and development of a new model of iodine-Epoxy paint interactions for PHEBUS and PWR severe accident applications", J. Radio. Nucl. Chem., 314 (2), p. 1121-1140 (2017) (https://dx.doi.org/10.1007/s10967-017-5458-9)

19 L. Bosland and J. Colombani, "Study of the radiolytic decomposition of CsI and CdI2 aerosols deposited on stainless steel, quartz and Epoxy painted surfaces", Annals of Nuclear Energy, 141, 107241 (2020) (https://dx.doi.org/10.1016/j.anucene.2019.107241)

20 L. T. Zhuravlev, "The surface chemistry of amouphous silica. Zhuravlev model", Colloids and Surfaces A: Physicochemical and Engineering Aspects 173: 1-38 (2000)

21 G.J. Evans, R.E. Jervis, "Radiochemical Studies of Iodine Behavior under Conditions Relevant to Nuclear Reactor Accidents", Journal of Radioanalytical and Nuclear Chemistry 161(1):121-133 (1992)

22 C. Farley and M. L. Pantoya, "Reaction kinetics of nanometric aluminum and iodine pentoxide", J. Therm. Anal. Calorim, 102, 609-613 (2010) (https://dx.doi.org/10.1007/s10973-010-0915-5)

23 H. Fjellvag and A. Kjekshus, "The crystal structure of I2O4 and its relations to other Iodine-oxygen containing compounds", Acta Chemica Scandinavia, 48, 815-822 (1994)

24 G. Daehlie, G. and A. Kjekshus, "Iodine oxides. Part I. On I2O3-SO3, I2O3-4SO3-H2O, I2O3-SeO3 and I2O4" Acta Chemica Scandinavia, 18, 144-156 (1964)

25 K. Selte, and A. Kjekshus, "Iodine oxides. Part II. On the system H2O-I2O5", Acta Chemica Scandinavia, 22, 3309-3320 (1968)

26 T. Wu, A. Sybing, et al., "Aerosol synthesis of phase pure iodine/iodic biocide microparticles", J. Mat. Res., 32(4): 890-896 (2017) (https://dx.doi.org/10.1557/jmr.2017.6)

27 B.K. Little, S.B. Emery, et al,. "Physiochemical characterization of Iodine(V) oxide, Part 1: hydration rates" Propellants Explos. Pyrotech. 35: 1-10 (2010) (https://dx.doi.org/10.1002/prep.201400225)

28 B.K. Little, S.B. Emery, et al., "Physicochemical characterization of Iodine (V) Oxide Part II: morphology and crystal structure of particulate films", Crystals 5: 534-550 (2015) (https://dx.doi.org/10.3390/cryst5040534)

29 J. C. Wren; G. A. Glowa and J. Meritt, "Corrosion of stainless steel by gaseous I2", J. Nucl. Materials, 265 p. 161-177 (1999)

30 G. Weber; L. Bosland; F. Funke; G. Glowa and T. Kanzleiter, "ASTEC, COCOSYS, and LIRIC Interpretation of the Iodine Behaviour in the Large-Scale THAI Test Iod-9", Proceedings of the 17th International Conference on Nuclear Engineering (ICONE 17), July 12th–16th, Brussels, Belgium, ICONE 17-75414, vol 2, 519-531 (2009)

31 P. Chatelard, S. Belon, L. Bosland, L. Carenini, L. Chailan, O. Coindreau, F. Cousin, C. Marchetto, H. Nowack, L. Piar, "Main modelling features of ASTEC V2.1 major version", Annals of Nuclear Energy, 93, p. 83-93, (2016) (https://dx.doi.org/10.1016/j.anucene.2015.12.026)

32 L. Bosland, F. Funke, and al., "PARIS project: Radiolytic oxidation of molecular iodine in containment during a nuclear reactor severe accident: Part 2: Formation and destruction of iodine oxides compounds under irradiation – experimental results modelling", Nucl. Eng. Des., 241, (9), p. 4026-4044, (2011) (https://dx.doi.org/10.1016/j.nucengdes.2011.06.015)

33 G. Weber; L. Bosland; F. Funke; G. Glowa and T. Kanzleiter, "ASTEC, COCOSYS, and LIRIC Interpretation of the Iodine Behavior in the Large-Scale THAI Test Iod-9", Journal of Engineering for Gas Turbines and Power, 132 (11) (2010) (https://dx.doi.org/10.1115/1.4001295)

34 L. Bosland; G. Weber; W. Klein-Hessling; N. Girault and B. Clement, "Modeling and interpretation of iodine behavior in PHEBUS FPT-1 containment with ASTEC and COCOSYS codes", Nucl. Tech., 177 (1), p. 36-62 (2012)